Reynolds-Stress Model for Eulerian multiphase

D. Cokljat*, M. Slack and S.A. Vasquez

Fluent Europe Ltd., Sheffield Business Park,
Europa Link, Sheffield S91 XU, UK
E-mail: davor@fluent.co.uk E-mail: mike@fluent.co.uk
E-mail: sav@fluent.co.uk
*Corresponding author

A. Bakker

Fluent Inc., 10 Cavendish Court,
Lebanon NH 03766, USA
E-mail: ab@fluent.com

G. Montante

Chemical Engineering Department,
University of Bologna, viale Risorgimento 2 – 40136 Bologna, Italy
E-mail: giusi.montante@mail.ing.unibo.it

Abstract: This paper presents a way of modelling turbulence in multiphase flows within the context of the Reynolds-Stress Model. The model has been implemented in the general-purpose unstructured finite volume code Fluent V6. Two multiphase turbulence approaches were considered: mixture and dispersed models. The mixture model solves the Reynolds-stress transport equations on the mixture level only. The dispersed approach solves the Reynolds-stress transport equations for the continuous phase, while the turbulence closure for the dispersed phases is achieved by an extension of the theory of dispersion of discrete particles by homogeneous turbulence. The dispersed model was used to calculate bubbly flow over a cylindrical back-step and the flow in an unbaffled stirred vessel. The mixture approach was used to calculate an industrially relevant cyclone flow.

Keywords: Eulerian multiphase; Reynolds-tress Model; RSM; turbulence modelling.

Reference to this paper should be made as follows: Cokljat, D., Slack, M., Vasquez, S.A., Bakker, A. and Montante, G. (xxxx) 'Reynolds-Stress Model for Eulerian multiphase', *Progress in Computational Fluid Dynamics*, Vol. x, No. x, pp.xxx–xxx.

Biographical notes: D. Cokljat received his PhD in Computational Fluid Dynamics, London in 1993 and his post Doctorate at City University, London in 1993–1994. From 1994–1996, he worked as a Higher Scientific Officer at Central Government Laboratory, Daresbury UK. Since 1996, he has been working as a Senior Principal Developer, Fluent Europe, UK. He was also a Visiting Lecturer, UMIST Manchester, UK since 2001–2002.

M. Slack received his Phd in Novel Cyclone Design in 1997. Since 1997, he has been working as a Prinicipal engineer, Fluent Europe. He was also a CFD application specialist for Oil and Gas and Chemical process industries.

S.A. Vasquez received his Phd in Turbulence Modelling from the University of Sheffield in UK. He has been working as a Development Fellow and Technical Lead in Multiphase Software Development in Fluent Europe in UK. He also worked on the development and application of numerical methods and physical methods for single and multiphase problems for over 20 years.

A. Bakker received his PhD in Applied Physics from Delft University of Technology, the Netherlands and his MBA in Technology Management from the University of Phoenics, USA. He has been working as a Product Manager with Fluent Inc. in the USA. His specialisation includes computational fluid dynamics in chemical engineering applications, including mixing processes and multiphase flow.

G. Montante received her PhD in Chemical Engineering from the University of Palermo in Italy. She is a Assistant Professor from the University of Bologna in Italy. Her research interests are currently focused on experimental and computational fluid dynamics of stirred vessels, with a special interest in multiphase flow.

1 Introduction

Owing to computational constraints, most practical applications of computational fluid dynamics (CFD) require the use of a turbulence closure model. CFD practitioners resolving single-phase turbulent flows have a number of different turbulence models available. The level of complexity of such models is strongly dependent upon the nature of the flow. For example, if turbulence anisotropy plays an important role within the flow structure, typically some form of Reynolds-Stress Model (RSM hereafter) is required in order to model it properly. Analogously to single-phase flows, there is no unique model that can predict all multiphase flows accurately. Modelling the effects of turbulence on mass and momentum transfer between phases is a difficult task and it is an ongoing research area. Turbulence models for multiphase flows not only have to deal with all complex modelling issues arising from the single phase turbulence, but also have to model additional generation and dissipation mechanisms that take into account the interaction between the phases. Typically these interactions may enhance or attenuate the continuous phase turbulence, which depends mainly on particle, bubble or droplet size and concentration. Nowadays, the industry standard for multiphase turbulence modelling is the use of two equation models, which are based on their single-phase counterparts. These models have several variants in order to deal with multiphase flows. Examples include a dispersed variant in which turbulence is solved only for the continuous phase and a phase coupled approach in which turbulence is solved for each phase separately (see Cokljat et al., 2000).

However, quite often the CFD practitioner may face a situation in which two-equation turbulence models cannot deal with the underlying flow physics (e.g., strongly anisotropic flows like cyclones and unbaffled stirred vessels). In such circumstances, additional turbulence modelling owing to multiphase flows does not play an important role anymore because the basic underlying single-phase model cannot deal with the complex physics of the flow. In such situations, the logical way forward is to combine RSM with a multiphase algorithm in order to be able to deal with those challenging situations in which both factors, RSM for turbulence and an Eulerian multiphase formulation, are preconditions for accurate predictions. This is a challenging task not only in terms of physical modelling but also in a numerical sense given the number of equations that need to be solved simultaneously (e.g., for 3d simulation of only two-phase system, 16 equations need to be solved). Consequently, there are very few articles on this subject available in the literature. To our knowledge, this article is the first report on results using RSM in conjunction with Euler-Euler multiphase models using an unstructured control volume methodology.

The main purpose of this paper is to report on the current state-of-the art in this area and on the progress made so far. After checking the model on a more academic test case (a back step flow), the primary intention of the following sections is to move on to more challenging, practical cases in order to critically review the model's ability to handle real-life, industrial-strength test cases. We have chosen the complex multiphase swirling flows in a hydrocyclone and in unbaffled stirred vessels as representative test cases, because it is well known that resolution of such flows using computational modelling techniques is not a trivial task.

2 Governing equations

The phase-averaged continuity and momentum equations for the phase 'k' read:

$$\frac{\partial}{\partial t}(\bar{\alpha}_k \rho_k) + \nabla \cdot (\bar{\alpha}_k \rho_k \tilde{U}_k) = 0 \tag{1}$$

$$\frac{\partial}{\partial t}(\bar{\alpha}_k \rho_k \tilde{U}_k) + \nabla \cdot (\bar{\alpha}_k \rho_k \tilde{U}_k \otimes \tilde{U}_k) = -\bar{\alpha}_k \nabla \tilde{p} + \nabla \cdot \tilde{\tau}_k^t + F_{Dc}. \tag{2}$$

In the above equations subscript 'k' is replaced by 'c' for continuous phase or 'd' for dispersed phases. Furthermore, the laminar stress–strain tensor and other body forces (e.g., gravity) are omitted for the sake of simplicity. The tilde denotes phase-averaged variables, while the overbar refers to time-averaged values. The phase turbulent stress tensor embodies all fluctuations including the so-called pseudo-turbulence. Phase averaging of any variable Φ and the fluctuation component are defined as:

$$\tilde{\Phi}_k = \frac{\overline{\alpha_k \Phi_k}}{\bar{\alpha}_k}, \quad \bar{\phi}'' = -\frac{\overline{\alpha_k \phi' k}}{\bar{\alpha}_k}. \tag{3}$$

The only momentum exchange force considered here is the drag force between the continuous and dispersed phases (only two phases are included here for clarity) and it is defined as:

$$F_{Dc} = K_{dc}\left[(\tilde{U}_d - \tilde{U}_c) - \left(\frac{\overline{\alpha_d u_d'}}{\bar{\alpha}_d} - \frac{\overline{\alpha_c u_c'}}{\bar{\alpha}_c}\right)\right]. \tag{4}$$

Here K_{dc} is a coefficient representing a characteristic density times an inverse time scale of the dispersed phase. Nearly all definitions of coefficient K_{dc} include a drag coefficient, and in this study we used Schiller-Nauman (Schiller and Naumann, 1935) model for that purpose. The time-averaged terms represent turbulent dispersion in the momentum equations. There are several terms in the above equations that need to be modelled in order to close the phase-averaged momentum equations. Full descriptions of all modelling assumptions are available in Cokljat et al. (2000). Here we concentrate only on the modelling tasks that are different compared to that study, namely the definition of the turbulent stresses $\tilde{\tau}_k^t$ that appear in Equation (2).

2.1 Turbulence modelling

Turbulent stresses appearing in the momentum equations need to be defined per-phase and are denoted as:

$$\tilde{\tau}_k^t = -\bar{\alpha}_k \rho_k \tilde{R}_{k,ij}. \tag{5}$$

Here the subscript k is replaced by c for the continuous phase or by d for any dispersed phase. Similar to its single-phase counterpart, the present multiphase RSM also solves transport equations for the Reynolds-stresses $\tilde{R}_{ij}$. Two methods for modelling turbulence in multiphase flows within the context of the RSM are presented in this study: dispersed and mixture turbulence models.

2.1.1 Dispersed model

The dispersed turbulence model is used when the dispersed phases are dilute, and in that case the continuous-phase turbulence is regarded as the dominant process. Consequently, transport equations for turbulence quantities are only solved for the continuous phase, while the predictions of turbulence quantities for dispersed phases are obtained using the well-known Tchen theory (Hinze, 1975). The transport equation for the continuous phase Reynolds stresses in the case of the dispersed model reads:

$$\begin{aligned}
&\frac{\partial}{\partial t}(\bar{\alpha}\rho\tilde{R}_{ij}) + \frac{\partial}{\partial x_k}(\bar{\alpha}\rho\tilde{U}_k\tilde{R}_{ij}) \\
&= -\bar{\alpha}\rho\left(\tilde{R}_{ik}\frac{\partial\tilde{U}_j}{\partial x_k} + \tilde{R}_{jk}\frac{\partial\tilde{U}_i}{\partial x_k}\right) + \frac{\partial}{\partial x_k}\left[\bar{\alpha}\mu\frac{\partial}{\partial x_k}(\tilde{R}_{ij})\right] \\
&\quad - \frac{\partial}{\partial x_k}\left[\bar{\alpha}\rho\overline{u_i'u_j'u_k'}\right] + \overline{\bar{\alpha}\, p\left(\frac{\partial u_i'}{\partial x_j} + \frac{\partial u_j'}{\partial x_i}\right)} - \bar{\alpha}\rho\tilde{\varepsilon}_{ij} + \Pi_{R,ij}.
\end{aligned} \tag{6}$$

All variables presented above are per continuous-phase (c) and this subscript is omitted for clarity. The last term in Equation (6), $\Pi_{R,ij}$ takes into account the interaction between the continuous and dispersed phase turbulence and for second order closure it can be written in this form:

$$\begin{aligned}
\Pi_{R,ij} = K_{dc}\Big[&\overline{u''_{c,j}}(\tilde{U}_{d,i} - \tilde{U}_{c,i}) + \overline{u''_{c,i}}(\tilde{U}_{d,j} - \tilde{U}_{c,j}) \\
&+ \overline{u''_{c,j}(u''_{d,i} - u''_{c,i})} + \overline{u''_{c,i}(u''_{d,j} - u''_{c,j})}\Big].
\end{aligned} \tag{7}$$

This term is the contribution from the particulate drag and contains additional particulate-fluid velocity covariance as well as volume fraction flux vectors. Closure of this term is still a challenge; here we have made a bold assumption of neglecting the anisotropy of the exchange term and simplifying it for a more tractable expression:

$$\Pi_{R,ij} = \frac{2}{3}\delta_{ij}\Pi_{kc}. \tag{8}$$

Here δ_{ij} is the Kronecker delta and Π_{kc} represents the modified version of the original model by Simonin and Viollet (1990):

$$\Pi_{kc} = K_{dc}(\tilde{k}_{dc} - 2\tilde{k}_c + \tilde{V}_{\text{rel}} \cdot \tilde{V}_{\text{drift}}). \tag{9}$$

Here $\tilde{k}_c$ represents the turbulent kinetic energy of the continuous phase, $\tilde{k}_{dc}$ is the continuous-dispersed phase velocity covariance, and finally, $\tilde{V}_{\text{rel}}$ and $\tilde{V}_{\text{drift}}$ stand for the relative and drift velocities, respectively. In order to achieve full closure, a transport equation for the turbulent kinetic energy dissipation rate $\tilde{\varepsilon}$ is required. When modelling the $\tilde{\varepsilon}$ equation, we have used Elghobashi (Elghobashi and Abou-Arab, 1983) model to account for an extra dissipation term owing to the turbulence transfer mechanism as reported in Cokljat et al. (2000) and will not be described here. However, for consistency it is important to stress that fluctuating quantities of the dispersed phases are given in the terms of the mean characteristics of the continuous phase. Following (Simonin and Viollet, 1990), the fluid-particle turbulence kinetic energy, the turbulent kinetic energy and turbulent viscosity for the dispersed phase are given as:

$$\tilde{k}_{dc} = 2\tilde{k}_c\left(\frac{b + \eta_{dc}}{1 + \eta_{dc}}\right) \tag{10}$$

$$\tilde{k}_d = \tilde{k}_c\left(\frac{b^2 + \eta_{dc}}{1 + \eta_{dc}}\right) \tag{11}$$

$$\nu_d^t = \frac{1}{3}\tilde{k}_{dc}\tau_{dc}^t + \left(\frac{2}{3}\tilde{k}_d - b\frac{1}{3}\tilde{k}_{dc}\right)\tau_{dc}^F. \tag{12}$$

Here b takes into account virtual mass effects (neglected in this paper), $\eta_{dc} = \tau_{dc}^t / \tau_{dc}^F$ the ratio between the Lagrangian integral time scale calculated along particle trajectories, τ_{dc}^t, and the characteristic particle relaxation time, τ_{dc}^F. Models for b, τ_{dc}^t and τ_{dc}^F are also given in reference Simonin and Viollet (1990).

2.1.2 Mixture model

The main assumption behind the mixture model is that all phases share the same turbulence field, which consequently means that the term $\Pi_{R,ij}$ in the Reynolds stress transport equations (Equation 6) is neglected. Apart from that change, the equations maintain the same form, but with phase properties and phase velocities being replaced with mixture properties and mixture velocities. For example, the mixture density is calculated as:

$$\rho_m = \sum_{i=1}^{N}\tilde{\alpha}_i\rho_i. \tag{13}$$

Furthermore, the mixture velocities are calculated as:

$$\tilde{U}_m = \frac{\sum_{i=1}^{N}\bar{\alpha}_i\rho_i\tilde{U}_i}{\sum_{i=1}^{N}\bar{\alpha}_i\rho_i}. \tag{14}$$

Here N is the number of phases.

3 Numerical method

An unstructured control-volume method is used, whereby the domain is subdivided into discrete control volumes and the integration of the equations is performed on the individual control volumes (Mathur and Murthy, 1997; Kim et al., 1998). All results presented in this study used the second order upwind-based discretisation scheme. The velocity components, pressure and all scalars are calculated at the centre of each control volume (collocated approach). The details of implementation of Reynolds-stress model into single-phase solver are given in Kim (2001). This technique is extended to multiphase flows, whereby a Phase-Coupled SIMPLE (PC-SIMPLE) algorithm is used to couple the pressure and the velocity fields (Vasquez and Ivanov, 2000). The phase-coupled discretised momentum equations can be expressed as:

$$(\overline{A}_p - \overline{R}_p)\vec{U}_p^{i,*} = \sum_{nb}^{n} \overline{A}_{nb}\vec{U}_{nb}^{i,*} - \Omega_p \frac{\partial p^*}{\partial x_i} + \vec{B}_p^{i,n} \tag{15}$$

$$\vec{U}^{i,*} = (U_1^{i,*}, U_2^{i,*}, \ldots, U_N^{i,*})^T, \quad \vec{\Omega} = \Omega(\alpha_1, \alpha_2, \ldots, \alpha_N)^T. \tag{16}$$

In the above equations, the velocities represent the phase vectors at the current iteration (as indicated by the asterisk *), whereby the superscript *i* refers to a physical vector component of each phase. The coefficients *A* are the matrices (with either subscript *p* for cell centre or subscript *nb* that stands for cell neighbours) that contain the influence from the transient, convection and diffusion terms. The $\overline{R}_p$ terms are matrices representing the momentum exchange terms. The pressure term is multiplied by the phase-volume vector, Ω_p, and the last term $\vec{B}_p^{i,n}$ in Equation (14) is a source representing body forces and linearised terms, whereby *n* refers to the previous iteration.

In the PC-SIMPLE algorithm, in order to avoid bias towards a heavy phase, the pressure correction needs to be based on the conservation of total volume. This is accomplished by using the following discretised form of the *N*-phase total volume continuity equation for incompressible fluids:

$$\sum_{f}^{n} \sum_{k=1}^{N} \alpha_{k,f}^{*} (\Theta_{k,f}^{*} + \Theta_{k,f}') = 0. \tag{17}$$

Here the subscript *f* refers to the cell face and *n* is the number of cell faces. The volume flux correction, $\Theta_{k,f}'$, is derived from the coupled momentum equations as:

$$\Theta_f' = -\frac{\vec{\Omega}_f}{(\overline{A}_p - \overline{K}_p)} \frac{\vec{A} \cdot \vec{A}}{\vec{A} \cdot \vec{ds}} (p_1' - p_0'). \tag{18}$$

Here, $\vec{A}$ is the face area vector between cells '0' and '1', while $\vec{ds}$ is the distance vector between the centroids of neighbouring cells. The pressure-correction is obtained by inserting Equation (18) into Equation (17).

4 Results

4.1 Flow over a cylindrical back-step

The first test case considered in this study is turbulent bubbly flow over a cylindrical back-step, which was studied experimentally by Bel'Fdhila (1991). The simulations were performed using the dispersed RSM turbulence model. This test case consists of two pipes with a sudden diameter change from 5 cm to 10 cm, respectively. The flow is fully developed at the inlet, and mass flow rates are available for both the continuous phase (water) and dispersed phase (air) there. Inlet Reynolds number based on liquid velocity is 39300 and bubble size was fixed to 2 mm. The calculations were performed using a two-dimensional axi-symmetric quadrilateral mesh consisting of 8800 cells, which was found to lead to the grid independent results (i.e., grid adaptation resulting in four times finer grid produced the results of negligible difference). Figure 1 presents results for the axial velocity at several locations downstream of the sudden expansion. Predictions were obtained using the standard k-ε model as well as RSM for the continuous phase, while the turbulence for the dispersed phase was approximated as reported in Cokljat et al. (2000). It is clear that both models produce similar results for the axial velocity. The trend of the RSM results suggests that the choice of the turbulence model makes a significant impact on the prediction of the dispersed phase volume fraction, as can be seen in Figure 2 (second row). The RSM successfully predicts the position of the measured volume fraction peaks at about $r/R = 0.5$. The observation that the choice of turbulence model makes a significant impact on the volume fraction distribution despite almost identical predictions of velocity field also was found in the work of Lathouwers (1999). In spite of the improvements, the RSM results are not entirely satisfying. It would remain to be seen in further studies if a better modelling of the volume fraction fluxes would capture the dispersion of the bubbles into the recirculation zone.

Figure 1 Axial velocity profiles in bubbly flow over a back-step

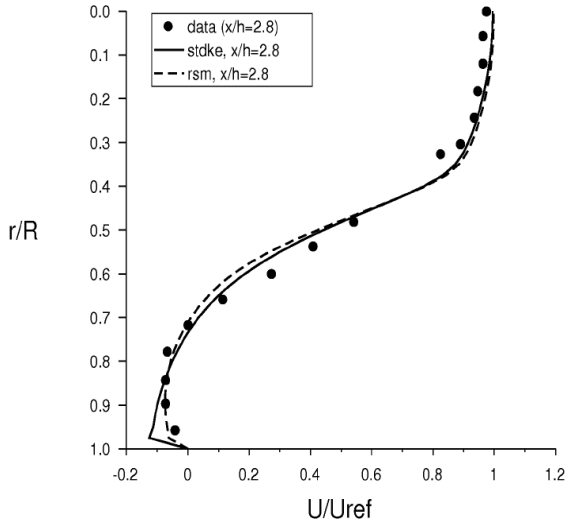

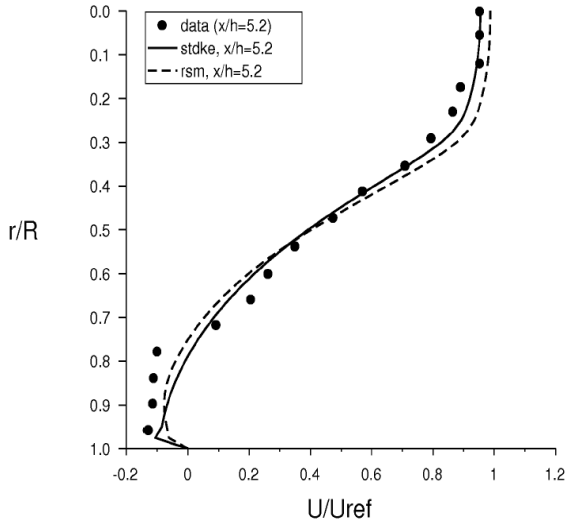

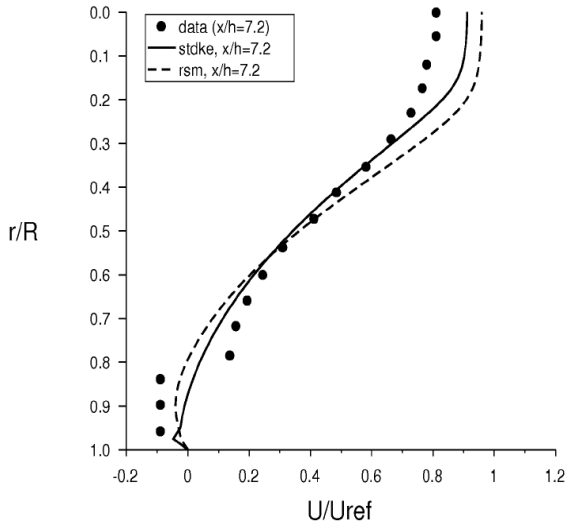

Figure 2 Air volume fraction in bubbly flow over a back-step

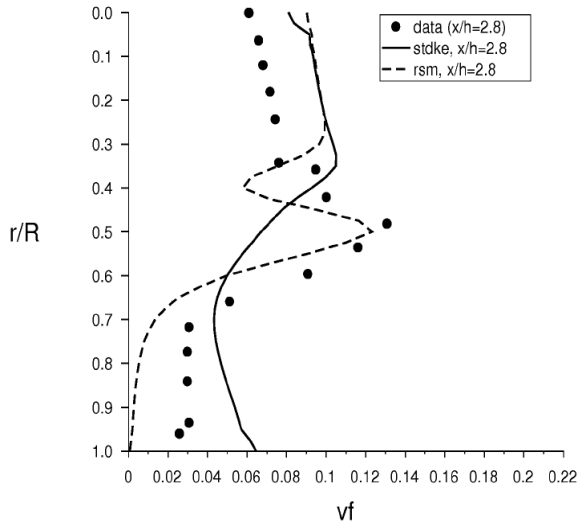

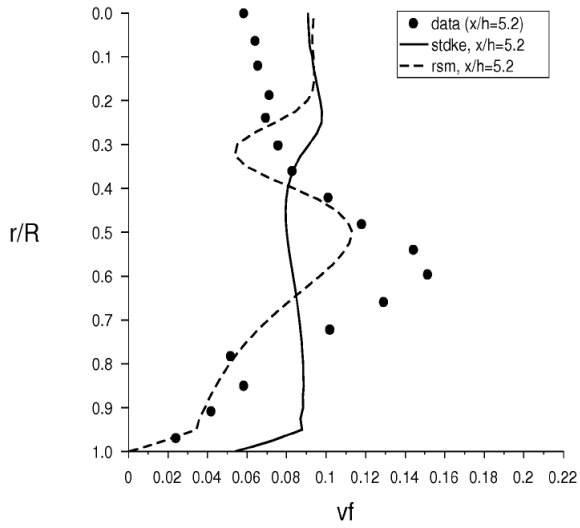

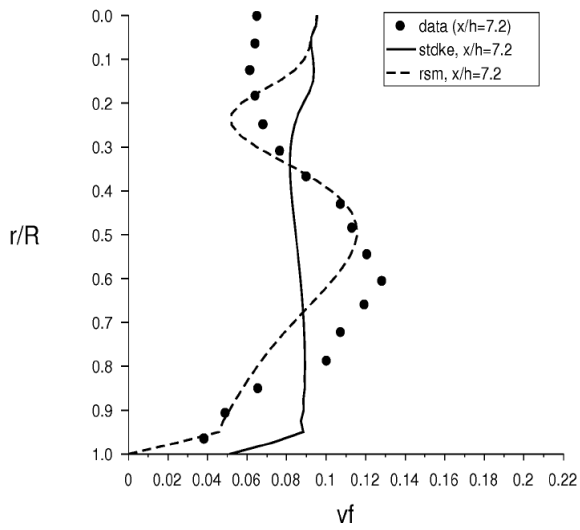

4.2 Flow in cyclones

The prediction of the flow behaviour inside cyclones is a challenging task. The correct choice of turbulence model is a critical factor in capturing the anisotropic turbulent features of this flow. Cyclones are used to separate or classify dispersed phases. The cyclone works by inducing spiral rotation in the continuous phase, and therefore imposes an enhanced radial acceleration on a particulate suspension (see Figure 3). In conventional cylindrical cyclone devices, there are two outlets, both on the axis of symmetry. The underflow is situated at the apex of the cone, and the overflow is an inner tube that descends from the top of the cyclone. The density of the suspended particulate phase is normally greater than the continuous phase. Owing to the imposed swirl, larger particles migrate radially to the outer wall and then spiral down to the underflow. Smaller particles migrate more slowly, are captured in an upward spiral in the centre of the cyclone and leave through the top via the vortex finder. Running liquid cyclones (commonly known as hydrocyclones) open to the atmosphere instead of closed, adds an additional complexity. Owing to the low pressure at the cyclone axis, a back-flow of gas can occur, which then forms a gas core as shown in Figure 5. Experimental work has shown that the tangential velocity increases sharply with radius in the central core region under the vortex finder, and thereafter it decreases with radius (Kelsall, 1952). This typical radial transition between a free and a forced vortex is demonstrated in Figure 5 (top). The constrained swirling flow field in a cyclone means that turbulent fluctuations are constrained in the tangential and axial directions but not in the radial direction. To accommodate this anisotropy of the turbulence, it is necessary to use a second order turbulence model. It is well known that this behaviour cannot be captured using traditional, eddy-viscosity, two-equation models (see Slack and Wraith, 1997 for further reference).

Figure 3 Cyclone separation process

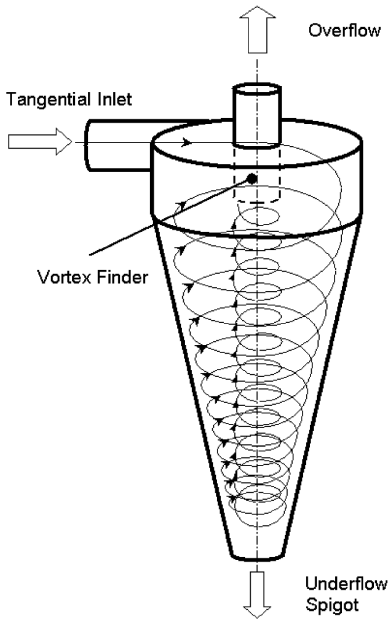

Most practical CFD modelling of cyclones has been limited to cases without an air core. Industrial cyclone modelling to date is limited to single phase flow calculations, and the separation efficiency is predicted using a Lagrangian particle tracking approach. In contrast, hydrocyclones commonly operate open to the atmosphere with slurry feed concentrations in excess of 10% by volume. By virtue of the nature of the system, the suspended second phase will be further concentrated within the device. The high second phase volume fractions that can occur in the model mean that Lagrangian and mixture modelling approaches are not suitable.

To correctly predict the flow split between the underflow and the overflow, it is necessary to account correctly for the shape of the air core. The low-pressure air core shape and size are functions of the swirling velocity field and the localised slurry density. It is necessary to resolve the strong coupling between the slurry concentrations, the swirl, and the resulting back flow of air, which forms the low-pressure air core. Modelling this multi-fluid, anisotropic turbulent system is a complicated industrial-strength challenge.

In the present work, a study of a hydrocyclone has been carried out using an Eulerian-Eulerian algorithm coupled with a full Reynolds-Stress Model. The Reynolds Stress transport equations were solved on the mixture level only. The study considered six phases: a continuous liquid phase, a gas phase that developed into an air core, and four granular phases of different particle sizes, which made up the slurry. In order to accommodate the complex tangential inlet shapes, we used a non-conformal meshing strategy as can be seen in Figure 4. The results presented in the following section extend the application of CFD to high and medium density cyclones.

Figure 4 Cyclone mesh

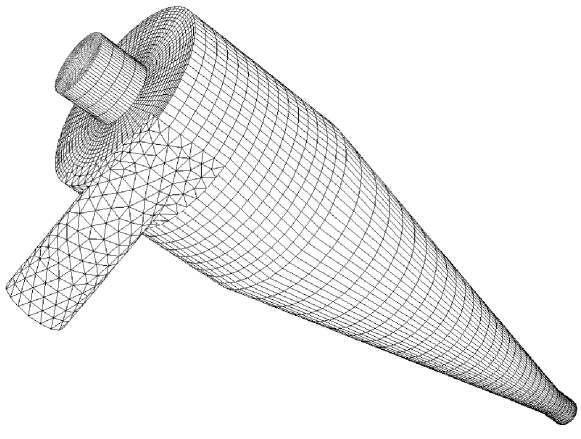

4.2.1 Results for hydrocyclones without solid feed

The results presented here have been compared against the published study by Monredon et al. (1990) and are calculated using a non-conformal three-dimensional mesh consisting of 180,000 cells, which we found to be sufficiently fine to ensure grid independent results for the flow in the cyclone considered in this study. The cyclone

considered here (Hydrocyclone No. 1 from the above study) is a 75 mm diameter hydrocyclone operating open to the atmosphere with a stable air core. The cyclone Reynolds number is 178500, and air bubble size is assumed to be 0.5 mm. Two different types of feed are considered: a pure water feed and a limestone and water slurry feed (10.47% w.r.t weight), whereby mass flow rates are 70.24 kg/min and 0.21 kg/min for water and solids, respectively. Further details of the experimental work are available in Monredon et al. (1990).

Figure 6 compares tangential velocity profiles measured at 50 mm and 120 mm depth (from the roof of the cyclone) for the water-only model. Experimentally, it is not possible to measure the local fluid velocity by LDA in slurries even as low as 1% by volume. Air is drawn in at the underflow and exits through the overflow via a stable air core. The model resolves the air core well at the apex; however, the clarity of the interface smudges slightly towards the overflow, as seen in Figure 5 (bottom). At this moment, it is not clear to the authors why the air core close to the vortex finder region is not as sharp as it is in the bottom half of the cyclones. Further work will be conducted in order to gain a better understanding of the problem. However, the free and forced vortex features are clearly captured.

Figure 5 Tangential velocity (top) and air volume fractions contours (bottom) in the cyclone

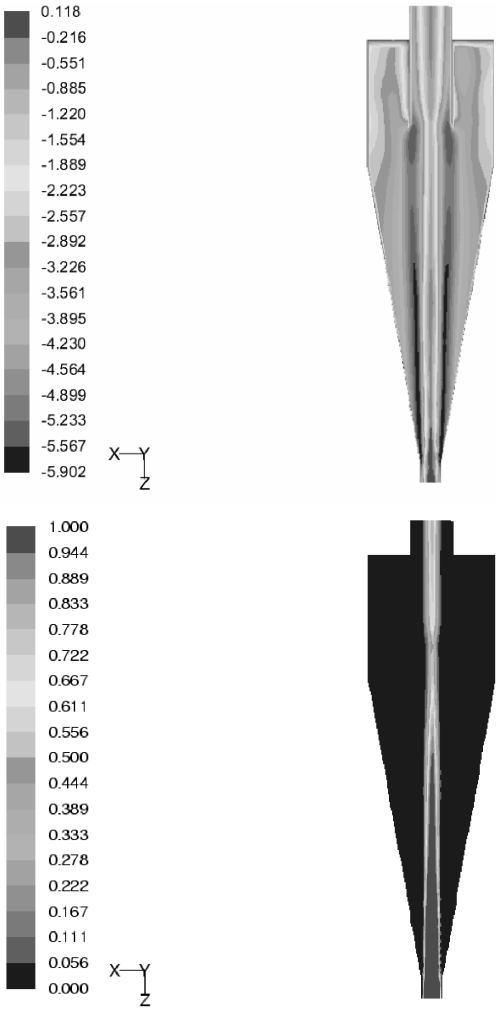

Figure 6 Tangential velocity profiles in the cyclone

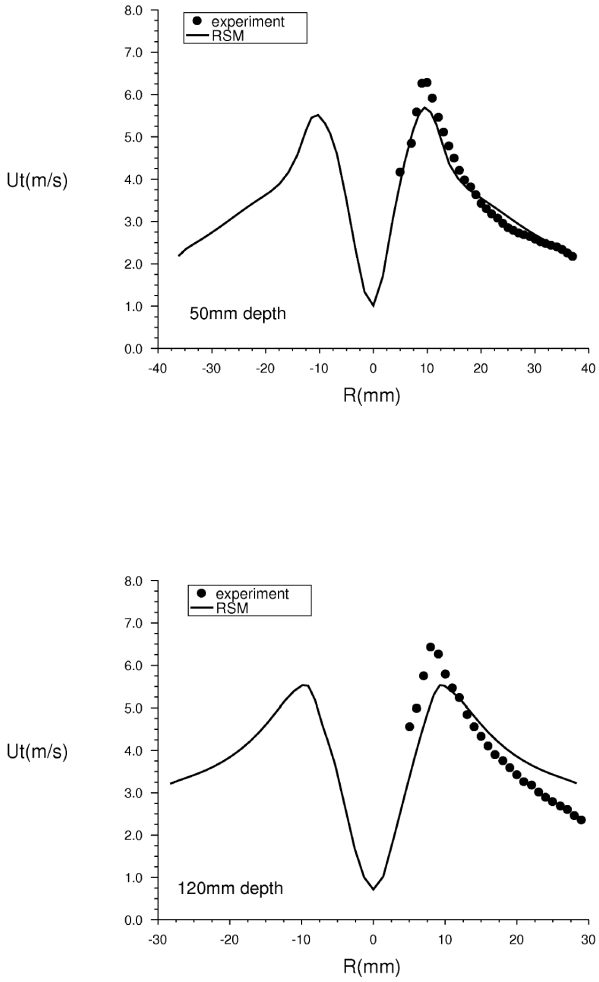

4.2.2 Results for hydrocyclones with solid feed

Next we move onto a simulation with limestone and water slurry feed. The opacity of the slurry means that for the 10.47% limestone slurry simulation, it is only possible to compare the separation performance of the device. Experimentally, six size bands have been measured to classify the separation performance of the hydrocyclone. The present model considers four limestone particle sizes. Comparison between the experiment and the prediction is shown in Figures 7 and 8. Fine particles experience a smaller radial force, and therefore they migrate more slowly to the conical wall of the cyclonic device. Figure 7 (top) shows how the 10 μm particles remain suspended in the water. The dark blue region in the plot shows the presence of the air core. The 10-μm particle size band reports to the underflow in a proportion similar to the flow split between the underflow and overflow, which is expected. In contrast, the 20 μm particles experience a higher radial force, and consequently, less material remains in suspension (Figure 7, bottom). Although not shown, the 30 μm and 40 μm particles are transported to the cyclone walls very quickly. Only a small fraction of the 30 and 40 μm size band does not leave via the underflow. The outstanding fraction is transported across the roof of the cylindrical section and down the vortex finder wall. This flow feature is known

as a short circuit path and results from the swirling flow in the top of the cyclone as it mixes with the inlet flow. The predicted separation efficiency follows the correct trend, as can be seen clearly in Figure 8. Considering the factors that can impact both the experimental measurement of slurry classification and the stability and sensitivity of this strongly swirling multiphase system, the results show that the model is fit for this type of analysis.

Figure 7 Particles (limestone) distribution within the cyclone

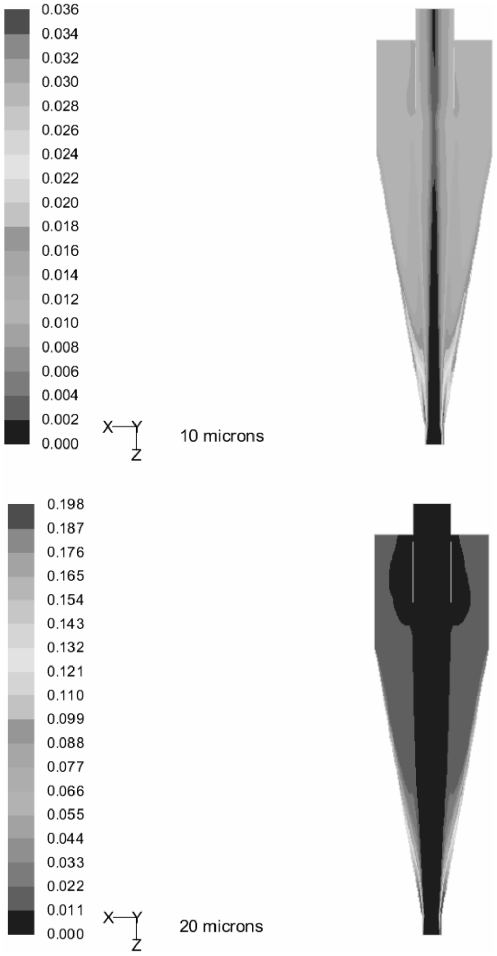

Figure 8 The cyclone separation efficiency curve for limestone particles

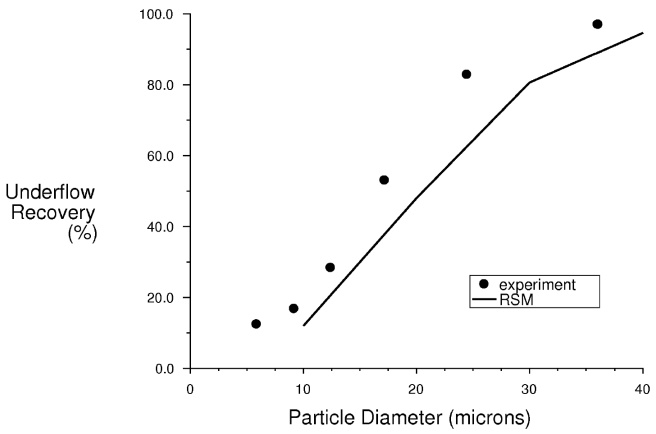

4.3 Flow in unbaffled stirred vessels

In the chemical and process industries, stirred vessels are commonly used to mix multiple dispersed phases. Examples regarding solid–liquid systems include crystallisers and chemical reactors where catalyst particles have to be evenly distributed throughout the liquid. Typical process vessels are cylindrical and have one or more impellers on a central shaft. For mixing of solid particulates, practical industrial design is usually done based on experimental correlations for the impeller speed at which particles are lifted off the vessel bottom. Such correlations do not provide information about the spatial distribution of the solids, which is of course an important variable when predicting reactor productivity. A significant amount of research has been performed to look into using multiphase flow CFD models to predict local solids concentrations, e.g., in Bakker et al. (1994) and Montante et al. (2000).

In most industrial vessels, vertical flat baffle plates are usually mounted on the vessel wall to improve mixing performance by converting tangential momentum into an axial, top-to-bottom motion. The use of baffles is not possible in all cases, however. In vessels without baffles, a strongly swirling flow develops, and mixing performance degrades. Eddy viscosity models have been used with reasonable success for fully baffled stirred tanks where the degree of swirl is low for both single-phase flow (Bakker et al., 1996) and multiphase flow systems (Montante et al., 2001). But from single-phase flow studies, it is known that eddy viscosity models are incapable of correctly predicting the swirling flows in unbaffled stirred tanks; see Ciofalo et al. (1996). The RSM is required for such systems.

For validation purposes, we studied two systems: an unbaffled vessel equipped with four radial pumping Rushton turbines, and the same vessel equipped with four down pumping A310 impellers. The experimental solids concentration data were published previously by Pinelli et al. (2001). The vessel diameter was 0.236 m. The vessel height was 0.944 m. The vertical concentration profile of glass particles with a diameter of 0.33 mm and a density of 2450 kg/m^3 was measured using an optical light attenuation technique. More details about the experiments can be found in Pinelli et al. (2001).

The first validation involves the four Rushton impellers. These impellers have six flat blades mounted on a disk. The outflow of the Rushton impeller is radial, with circulation loops forming above and below each impeller. There is little overall top-to-bottom motion, and there is significant segregation between the various circulation loops. The average solids concentration for this test was 2 kg/m^3. The impeller diameter was one-third of the vessel diameter, and the rotational speed was 17.9 s^{-1}. The liquid viscosity was 0.0057 Pa-s. The impeller Reynolds number was 20,000. The simulations were performed using the dispersed RSM coupled with Eulerian granular multiphase model. Second order upwind differencing was used for

all variables. The Schiller-Nauman drag law was used (Schiller and Naumann, 1935). The turbulence correction to this drag law recommended by Pinelli et al. (2001) was found to be negligible for this particular case. A steady-state flow field and solids distribution were calculated, where the impellers were modelled using a multiple reference frame approach. Because of the periodic nature of the geometry, only a 60-degree section was modelled using a hexahedral mesh of 80000 cells.

To quantify the magnitude of the swirl relative to the other velocity components, the volume averages of the various predicted velocity components were calculated. The volume averaged tangential velocity in this system was 1.75 m/s, the volume averaged absolute axial velocity was 0.097 m/s and the volume averaged absolute radial velocity was 0.063 m/s. These results confirm that this flow is swirl-dominated.

Figure 9 shows the local volume fraction in a cross section of the vessel. The poor mixing performance of this system is apparent. As a result of the segregated circulation patterns, most of the solids stay below the bottom impeller. The solids fraction near the upper impellers is much lower. Figure 10 shows a comparison between the experimental data from Pinelli et al. (2001) and our model predictions. The normalised axial coordinate z/H is plotted on the y-axis, and the average solids concentration at that elevation is plotted on the x-axis. A good comparison is achieved, providing additional validation of the model.

Figure 9 The local volume fraction of solids in a cross section of a vessel equipped with four Rushton turbines, as predicted using RSM

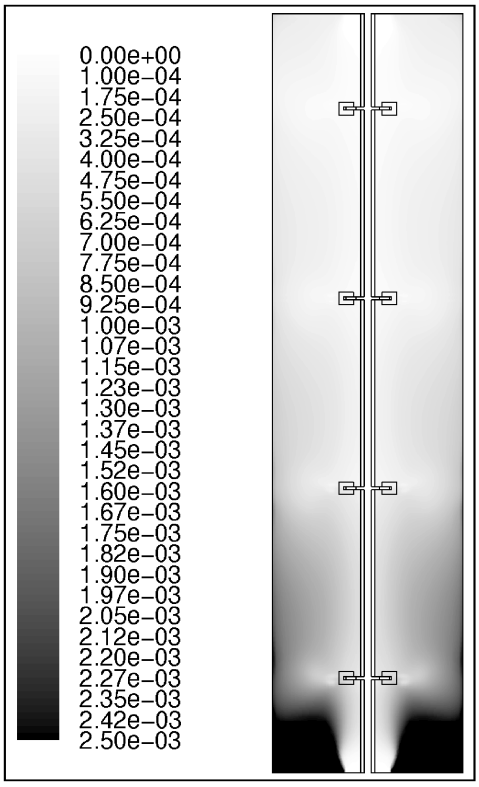

Figure 10 A comparison between experimental data from Montante et al. (2001) and predictions using the Reynolds stress model for an unbaffled stirred vessel equipped with four Rushton impellers. The normalised local solids concentration in the vessel C/C_{av} is plotted on the x-axis, and related to the normalised axial coordinate z/H on the y-axis

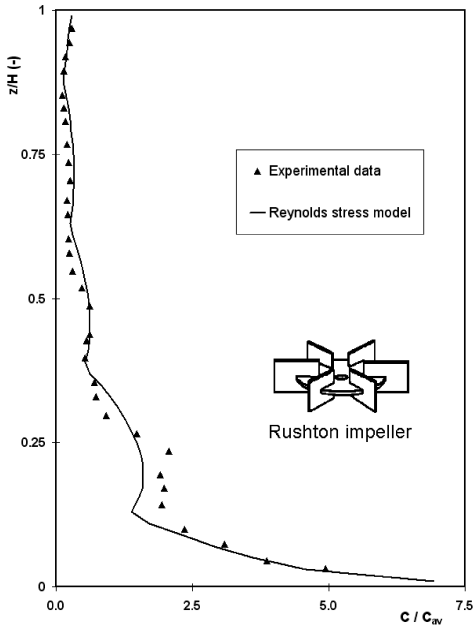

The second stirred tank validation involves the same vessel, but now equipped with four A310 hydrofoil impellers. The impeller diameter was 0.4 times the vessel diameter. The liquid was water. The impeller rotational speed was 16.6 s^{-1}, and the impeller Reynolds number was 80,000. The average solids concentration was 1.3 kg/m^3. To quantify the magnitude of the swirl relative to the other velocity components for this system, the volume averages of the various predicted velocity components were calculated. The volume averaged tangential velocity in this system was 0.70 m/s, the volume averaged absolute axial velocity was 0.22 m/s and the volume averaged absolute radial velocity was 0.12 m/s. These results confirm that this flow is also swirl-dominated, although the swirl is less strong for the A310 impellers than for the Rushton impellers.

Figure 11 shows the local volume fraction in a cross section of the unbaffled vessel equipped with four A310 impellers. Because of the periodic nature of the flow, only a 120-degree section of the vessel was modelled, using an unstructured hexahedral mesh of 1.1 million cells. The Schiller-Nauman drag law was used, and we applied the turbulent drag coefficient correction suggested by Pinelli et al. (2001).

In the multiple A310 system, most of the solids are eventually transported upwards, and get caught in a circulation loop in the upper part of the vessel. This phenomenon was also observed experimentally (Pinelli et al., 2001). Previously reported simulations using the RNG k-ε model failed to capture this behaviour (Montante and Magelli, 2003). Figure 12 shows

a comparison between the experimental data from Pinelli et al. (2001), the RNG k-ε results (Montante and Magelli, 2003) and our current RSM predictions. The normalised axial coordinate z/H is plotted on the y-axis, and the average normalised solids concentration at that elevation is plotted on the x-axis. It is obvious that the predictions using the RNG k-ε model do not match the experimental data at all. But a much better comparison is achieved between the RSM results and the experimental data, providing additional validation of the new model.

Figure 11 The local volume fraction of solids in a cross section of an unbaffled vessel equipped with four A310 impellers as predicted using a Reynolds stress model

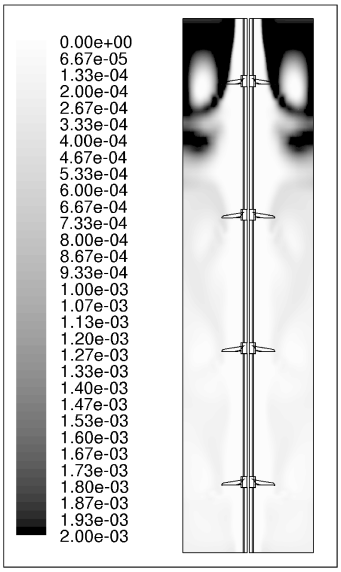

Figure 12 A comparison between experimental data from Montante et al. (2001), predictions using the RNG k-ε model (Pinelli et al., 2001), and the Reynolds stress model for an unbaffled stirred vessel equipped with four A310 impellers. The normalised local solids concentration in the vessel C/C_{av} is plotted on the x-axis, and related to the normalised axial coordinate z/H on the y-axis

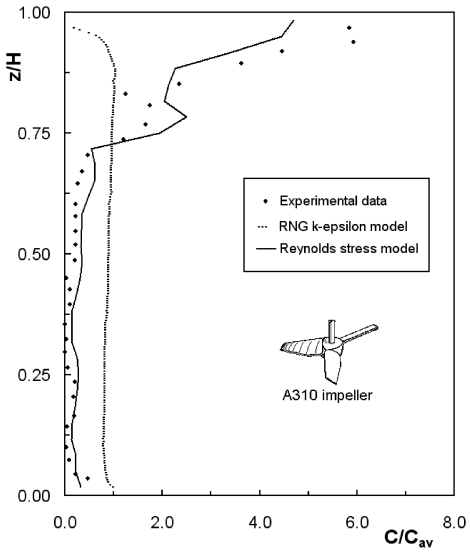

5 Conclusions

A full Reynolds-Stress Model of turbulence was implemented into the general-purpose CFD solver Fluent V6 in conjunction with an Euler-Euler multiphase algorithm. Two different multiphase turbulence approaches were considered: dispersed model in which Reynolds-stress equations are solved only for continuous phase, and mixture model in which turbulence equations are solved on mixture level. In order to make dispersed Reynolds Stress Model more robust for industrial type applications, the interaction term between continuous and dispersed phase turbulence was approximated so that only the normal stresses participate in the fluctuational energy exchange. In the case of mixture approach, further approximation was done for the hydrocyclone calculations by neglecting the exchange term in the RSM equations. Initial testing performed on three challenging industrial strength problems indicates superiority of this modelling approach for a variety of multiphase applications over more traditional approaches in which turbulence for multiphase applications is modelled using two-equation, eddy-viscosity models. In particular, the RSM model was able to capture measured volume fraction peaks in the case of cylindrical back step, to capture correct flow field in the case of hydrocyclone and finally to capture very accurately solid concentration in the stirred vessel equipped with the Rushton impeller. This work extends the application of CFD and will assist the design of unbaffled stirred vessels and medium and high slurry density hydrocyclones.

Acknowledgements

The authors wish to thank F. Magelli and his coworkers from the University of Bologna for providing useful advice and for making available the experimental data used in the unbaffled stirred tank validations. We also thank B. Gigas from Lightnin for making available the A310 impeller geometry.

References

Bakker, A., Fasano, J.B. and Myers, K.J. (1994) 'Effects of flow pattern on the solids distribution in a stirred tank', *8th European Conference on Mixing*, 21–23 September, Cambridge, UK, IChemE Symposium Series No. 136, ISBN 0 85295 329 1, pp.1–8.

Bakker, A., Myers, K.J., Ward, R.W. and Lee, C.K. (1996) 'The laminar and turbulent flow pattern of a pitched blade turbine', *TransIChemE*, Vol. 74, Part A., May, pp.485–491.

Bel'Fdhila, R. (1991) *PhD Thesis*, University of Toulouse, France.

Ciofalo, M., Brucato, A., Grisafi, F. and Torraca, N. (1996) 'Turbulent flow in closed and free-surface unbaffled tanks stirred by radial impellers', *Chem. Eng. Sci.*, Vol. 50, pp.3557–3573.

Cokljat, D., Ivanov, V.A., Sarasola, F.J. and Vasquez, S.A. (2000) 'Multiphase *k*-epsilon models for unstructured meshes', ASME paper FEDSM2000-11282, *Proceedings of ASME FEDSM 2000: ASME 2000 Fluids Engineering Division Summer Meeting*, Boston USA.

Elghobashi, S.E. and Abou-Arab, T.W. (1983) 'A two-equation turbulence model for two-phase plows', *Physics of Fluids*, Vol. 26, pp.931–938.

Hinze, J.O. (1975) *Turbulence*, 2nd ed., McGraw-Hill Publishing Co., New York, pp.460–471, ISBN 0-07-029037-7.

Kelsall, D.F. (1952) 'A study of the motion of solid particles in a hydraulic cyclone', *TransIChemE*, Vol. 30, pp.87–108.

Kim, S.E. (2001) *Unstructured Mesh Based Reynolds Stress Transport Modeling of Complex Turbulent Shear Flows*, AIAA Paper 2001-0728.

Kim, S.E., Mathur, S.R., Murthy, J.Y. and Choudhury, D. (1998) *A Reynolds-Averaged Navier-Stokes Solver Using Unstructured Mesh-Based Finite-Volume Scheme*, AIAA Paper 98-0231.

Lathouwers, D. (1999) *Modeling and Simulation of Turbulent Bubbly Flow*, PhD Thesis, Delft University of Technology, Delft, The Netherlands.

Mathur, S.R. and Murthy, J.Y. (1997) 'A pressure based method for unstructured meshes', *Numerical Heat Transfer*, Vol. 31, pp.195–216.

Monredon, T.C., Hsieh, K.T. and Rajamani, R.K. (1990) 'Fluid flow model of the hydrocyclone: an investigation of device dimensions', *Int. J. Miner. Process.*, Vol. 35, pp.65–83.

Montante, G. and Magelli, F. (2003) 'CFD predictions of solid concentration distributions in baffled and unbaffled vessels agitated with multiple A310 Impellers', *Proceedings of the Sixth Italian Conference on Chemical and Process Engineering*, June, Pisa, Italy, pp.1481–1486.

Montante, G., Micale, G., Brucato, A. and Magelli, F. (2000) 'CFD simulation of particle distribution in a multiple-impeller high-aspect-ratio stirred vessel', in van den Akker, H.E.A. and Derksen, J.J. (Eds.): *Proceedings 10th Europ. Conf. Mixing*, Delft, 2–5 July, Elsevier, Amsterdam, The Netherlands, pp.125–132.

Montante, G., Micale, G., Magelli, F. and Brucato, A. (2001) 'Experiments and CFD predictions of solid particle distribution in a vessel agitated with four pitched blade turbines', *Chem. Eng. Res. Des.*, Vol. 79, pp.1005–1010.

Pinelli, D., Nocentini, M. and Magelli, F. (2001) 'Solids distribution in stirred slurry reactors: influence of some mixer configurations and limits to the applicability of a simple model for predictions', *Chem. Eng. Comm.*, Vol. 118, pp.91–107.

Schiller, L. and Naumann, Z. (1935) 'A drag coefficient correlation', *Z. Ver. Deutsch. Ing.*, Vol. 77, p.318.

Simonin, C. and Viollet, P.L. (1990), 'Predictions of an oxygen *droplet* pulverization in a compressible subsonic coflowing hydrogen flow', *Numerical Methods for Multiphase Flows*, FED-Vol. 91, pp.65–82.

Slack, M.D. and Wraith, A.E. (1997) 'Modelling the velocity distribution in a hydrocyclone', *4th International Colloquium on Process Simulation*, pp.65–83.

Vasquez, S.A. and Ivanov V.A. (2000) 'A phase-coupled method for solving multiphase problems on unstructured meshes', *Proceedings of ASME FEDSM 2000: ASME 2000 Fluids Engineering Division Summer Meeting*, 11–15 June, Boston, Massachusetts.

Notations

Variables	
$\bar{\bar{A}}_p$	Coefficient matrices
$\vec{A}$	Face area vector
$a_{dc,i}$	Relative velocity (m s^{-1})
$\vec{B}_p^{i,n}$	Body forces and linearised terms
b	Virtual mass model constant (-)
$b_{dc,j}$	Drift velocity (m s^{-1})
$C_{1,dc}$	Model constant (-)
$C_{2,dc}$	Model constant (-)
C/C_{av}	Local solids concentration normalised by the vessel average concentration (kg m^{-3})
$\vec{ds}$	Distance vector between neighbouring cells
F_{Dc}	Drag force per volume (kg m^{-2} s^{-2})
H	Vessel height (m)
$\tilde{k}$	Turbulent kinetic energy (m^2 s^{-2})
K_{dc}	Drag coefficient (-)
N	Number of phases (-)
p	Pressure (Pa)
$\tilde{R}_{ij}$	Reynolds stresses (Pa)
R_p	Momentum exchange terms
U	Velocity (m s^{-1})
u'	Fluctuating velocity component (m s^{-1})
$\tilde{V}_{\text{rel}}$	Relative velocity (m s^{-1})
$\tilde{V}_{\text{drift}}$	Slip velocity (m s^{-1})
x_i	Coordinate (m)
z	Axial coordinate in the stirred vessel (m)
α	Volume fraction (-)
δ_{ij}	Kronecker delta (-)
$\tilde{\varepsilon}$	Turbulent energy dissipation rate (m² s^{-3})
Φ	General scalar variable
η_{dc}	Time scale ratio (-)
Ω_p	Phase-volume vector
Π_k	Model approximation of $\Pi_{R,ij}$ (kg m^{-1} s^{-3})
$\Pi_{R,ij}$	Turbulent phase-interaction Reynolds stress source (kg m^{-1} s^{-3})
$\Theta'_{k,f}$	Volume flux correction
ρ	Density (kg m^{-3})
$\tilde{\tau}^t$	Turbulent shear stresses (Pa)
τ^t_{dc}	Characteristic particle relaxation time (s)
τ^F_{dc}	Lagrangian integral time scale (s)
Subscripts	
c	Referring to continuous phase
d	Referring to dispersed phase
i	Index
f	Referring to cell face
k	Referring to phase k
m	Referring to the mixture
nb	Referring to neighbouring cells
p	Referring to cell centre